J|A|C|S ARTICLES

Published on Web 11/13/2009

Synthesis, Characterization, and Hierarchical Organization of Tungsten Oxide Nanorods: Spreading Driven by Marangoni Flow

Aswani Yella,[†] Muhammad Nawaz Tahir,[†] Stefan Meuer,[‡] Rudolf Zentel,[‡] Rüdiger Berger,[§] Martin Panthöfer,[†] and Wolfgang Tremel*,[†]

Institut für Anorganische Chemie und Analytische Chemie, and Institut für Organische Chemie, Johannes Gutenberg-Universität, Duesbergweg 10-14, D-55099 Mainz, Germany, and Max-Planck-Institut für Polymerforschung, Ackermannweg 10, D-55128 Mainz, Germany

Received January 30, 2009; E-mail: tremel@uni-mainz.de

Abstract: Tungsten oxide nanorods were synthesized by a soft chemistry approach using tungsten alkoxide and trioctyl amine and oleic acid as the surfactants. The optical properties of the nanorods were studied. The nanorods were found to be soluble in a wide range of solvents like chloroform, cyclohexane, and so on. Upon solvent evaporation, the nanorods formed hierarchically organized solid state structures. Depending on the solvent used, the nanorods organized in different mesostructures. Moreover, the organization of the nanorods from mixtures of polar and nonpolar solvents was studied. Here, the Marangoni effect resulting from differences in the surface tensions of the two solvents was found to play a role in the organization of the nanorods. Furthermore, dip coating of the nanorod solutions on a mica substrate resulted in the formation of a uniform thin film of the nanorods, which may be useful for a variety of applications such as in electrochromic devices and in organic light emitting devices (OLEDs) using tungsten oxide as a buffer layer.

Introduction

Self-assembly is a fundamental phenomenon that generates structural organization on all length scales. Among the variety of objects that can self-assemble into ordered structures, uniform spheres are the simplest model system. Ordering of spherical particles has been extensively studied both theoretically and experimentally.[1−3] Ordered self-assembly of anisotropic nanocrystals, such as nanorods (NRs), is more complicated than that of spheres due to their lower shape symmetry. Onsager[4] was the first to show theoretically that hard rods at very low volume fractions can form a distinct anisotropic phase with positional disorder and long-range orientational order (i.e., the nematic phase). Generally the formation of lyotropic liquid crystals[5−7] from rigid-rod objects as a result of form-anisotropy is well understood. Historically, lyotropic LC phases in water have been observed for various rigid-rod objects like V_2O_5 ribbons,[8,9] tobacco mosaic viruses,[10] and TiO_2 or WO_3 nanorods.[11] Significant progress has been made recently both on the synthesis of nanorods of different materials[12−14] as well as on understanding and mastering their assembly.[15−17] This can be mediated for instance by external fields,[18−23] by interparticle interactions as well as rod solubility in a binary solvent/nonsolvent liquid mixture,[23−25] by controlling the rod interfacial energy,[26] by slow solvent evaporation at the liquid−solid−air interface,[27] by solvent fluidics and the presence of liquid−air

[†] Institut für Anorganische Chemie and Analytische Chemie.
[‡] Institut für Organische Chemie.
[§] Max-Planck-Institut für Polymerforschung.

(1) Alder, B. J.; Hoover, W. G.; Young, D. A. *J. Chem. Phys.* **1968**, *49*, 3688–3696.
(2) Bolhuis, P. G.; Frenkel, D.; Mau, S.-C.; Huse, D. A. *Nature* **1997**, *388*, 235–236.
(3) Rudd, R. E.; Broughton, J. Q. *Phys. Rev. B* **1998**, *58*, 5893–5902.
(4) Onsager, L. *Ann. N. Y. Acad. Sci.* **1949**, *51*, 627–659.
(5) (a) Ballauff, M. *Angew. Chem.* **1989**, *101*, 261−273; *Angew. Chem., Int. Ed.* **1989**, *101*, 253−267. (b) Noël, C.; Navard, P. *Prog. Polym. Sci.* **1991**, *16*, 55–110. (c) Davidson, P.; Gabriel, J. C. P. *Curr. Opin. Colloid Interface Sci.* **2005**, *9*, 377–383.
(6) (a) Flory, P. J. *Proc. R. Soc. A* **1956**, *254*, 73–78. (b) Flory, P. J.; Ronca, G. *Mol. Cryst. Liq. Cryst.* **1979**, *54*, 289–310.
(7) Petekidis, G.; Vlassopoulos, D.; Fytas, G.; Kountourakis, N. *Macromolecules* **1997**, *30*, 919–931.
(8) (a) Zocher, H. *Z. Anorg. Allg. Chem.* **1925**, *147*, 91–110. (b) Brunello, C. A.; Graeff, C. F. O. *J. Non-Cryst. Solids* **2002**, *304*, 265–270.
(9) Bawden, F. C.; Pirie, N. W.; Bernal, J. D.; Fanhucken, I. *Nature* **1936**, *138*, 1051–1052.
(10) Dessombz, A.; Chiche, D.; Davidson, P.; Panine, P.; Chanéac, C.; Jolivet, J.-P. *J. Am. Chem. Soc.* **2007**, *129*, 5904–5909.
(11) (a) Michot, L. J.; Bihannic, I.; Maddi, S.; Baravian, C.; Levitz, P.; Davidson, P. *Langmuir* **2008**, *24*, 3127–3139. (b) Wang, J.; Khoo, E.; Lee, P. S.; Ma, J. *J. Phys. Chem. C* **2008**, *112*, 14306–14312.
(12) Hao, E.; Schatz, G. C.; Hupp, J. T. *J. Fluoresc.* **2004**, *14*, 331–341.
(13) Jun, Y. W.; Lee, J. H.; Choi, J. S.; Cheon, J. *J. Phys. Chem. B* **2005**, *109*, 14795–14806.
(14) Kumar, S.; Nann, T. *Small* **2006**, *2*, 316–329.
(15) Jana, N. R. *Angew. Chem.* **2004**, *116*, 1562−1566; *Angew. Chem., Int. Ed.* **2004**, *43*, 1536−1540.
(16) Ghezelbash, A.; Koo, B.; Korgel, B. A. *Nano Lett.* **2006**, *6*, 1832–1836.
(17) Titov, A. V.; Kral, P. *Nano Lett.* **2008**, *8*, 3605–3612.
(18) Harnack, O.; Pacholski, C.; Weller, H.; Yasuda, A.; Wessels, J. M. *Nano Lett.* **2003**, *3*, 1097–1099.
(19) Ryan, K. M.; Mastroianni, A.; Stancil, K. A.; Liu, H. T.; Alivisatos, A. P. *Nano Lett.* **2006**, *6*, 1479–1482.
(20) Gupta, S.; Zhang, Q.; Emrick, T.; Russell, T. P. *Nano Lett.* **2006**, *6*, 2066–2069.
(21) Hu, Z.; Fischbein, M. D.; Querner, C.; Drndic, M. *Nano Lett.* **2006**, *6*, 2585–2591.
(22) Nobile, C.; Fonoberov, V. A.; Kudera, S.; Della Torre, A.; Ruffino, A.; Chilla, G.; Kipp, T.; Heitmann, D.; Manna, L.; Cingolani, R.; Balandin, A. A.; Krahne, R. *Nano Lett.* **2007**, *7*, 476–479.
(23) Li, L. S.; Walda, J.; Manna, L.; Alivisatos, A. P. *Nano Lett.* **2002**, *2*, 557–560.

 10.1021/ja9007479 CCC: $40.75

interface in the deposition of a lyotropic phase from a drying solution,[27,31a] by a Langmuir−Blodgett approach,[28,29] or by unidirectional alignment through attachment of nanorods to the surface of a single cleaved semiconductor monolayer.[30] Important requirements for organizing nanorods in ordered close-packed arrays over large areas, however, are good shape homogeneity and, in the case of alignment assisted by external biases, the ability of nanorods to respond to such biases effectively.

Although reports on the self-assembly and liquid crystalline ordering in the case of polymer-coated metal oxide nanorods[31a−c] and carbon nanotubes[31d] have appeared, the liquid crystalline behavior of nonpolymer-coated metal oxide nanorods, especially of tungsten oxide, is not well understood. Among various other metal oxides, tungsten oxide has found useful applications in electrochromic devices,[32] semiconductor gas sensors,[33] and photocatalysis.[34] The Na_xWO_3 bronze is also reported to be a high temperature superconductor with a T_c of nearly 90 K.[35] In addition, nanostructured tungsten oxide has been used as a structure-directing precursor for WS_2 nanotubes,[36] a material that proved useful in tribological applications and catalysis. The morphology of the oxide nanorods is directly transferred to the resulting WS_2 nanotube after reaction with H_2/H_2S. To date, many methods have been deployed to prepare WO_3 in the form of powders, thin films, or colloidal solutions, including, for example, sol−gel chemistry, thermal oxidation of tungsten, thermal or electron beam evaporation, sputtering, spray pyrolysis, pulsed laser deposition, chemical vapor deposition, and electrodeposition.[37]

Here we report a facile soft chemistry route for the production of highly uniform, ultra narrow (2 nm) single-crystal tungsten oxide nanorods, 10 nm in length, with tight control over their diameter and their self-assembly behavior. To our knowledge, this is the first approach to synthesize highly homogeneous tungsten oxide nanorods, completely soluble in organic solvents and their assembly to form different superstructures by direct chemical synthesis. The ultra narrow diameter of the wires is apparent also from their absorption and photoluminescence (PL) behavior. We further demonstrate controlled assembly of the nanorods into 2D ultrahigh-density nanowire arrays over areas of several millimeters.

Experimental Section

Synthesis. In a typical synthesis of nanorods, tungsten ethoxide was decomposed in the presence of a mixture of trioctyl amine and oleic acid in a 1:1 ratio. The mixture of the surfactants was heated to 350 °C under inert atmosphere. The tungsten ethoxide solution was injected quickly into the flask at 350 °C, which was kept at this temperature for another 5 min before removing the heating mantle. Immediately after injection, the color of the solution changed to dark blue. The nanorods were precipitated by adding 15 mL of ethanol. The product was collected by centrifugation, thoroughly washed with ethanol, and dried at 60 °C. The yield was about 80%.

Characterization. The phase analysis of the products was carried out using powder X-ray diffraction (XRD) on a Bruker D8 Discover X-ray diffractometer with a 2D HiStar detector using Cu Kα radiation (λ = 1.5418 Å). The sizes and morphologies of the nanocrystals and films were measured using a JEOL JEM-1200EX transmission electron microscope (TEM) at 120 kV, a Tecnai G2 F20 S-Twin high-resolution transmission electron microscope (HRTEM) at 200 kV, and a JEOL JSM-6700F scanning electron microscope (SEM) at 10 kV. UV−vis absorption spectra were measured on a Hitachi U-3010 spectrophotometer. PL spectra were recorded with a Hitachi F-4500 fluorescence spectrophotometer. Samples for scanning force microscope (SFM) investigations were prepared by drop casting: one drop from a 100 μL syringe of sample solution was deposited on a freshly cleaved mica surface. All SFM images were recorded at room temperature under ambient conditions with a commercial SFM (Multimode, Nanoscope IIIa controller, Veeco, California) in tapping mode. This instrument was equipped with a piezoelectric scanner allowing a maximum x,y-scan size of 17 μm and a maximum z-extension of 3.9 μm. Silicon cantilevers (OMCL-AC240TS (Olympus), 240 μm long, 30 μm wide, 2.8 μm thick) with an integrated tip, a nominal spring constant of 2 N/m and 42 N/m, a tip radius <10 nm, and nominal resonance frequencies of 70 and 300 kHz were plasma cleaned prior to used. Typically the tip was scanned at velocities from 0.5 to 1 μm s^{-1}. For all samples the topography and phase contrast images were recorded. Raw data were modified by applying the first order "flatten" filter to achieve scan lines at the same average height and average tilt.

Results and Discussion

Structure of the $W_{18}O_{49}$ Nanorods. The dark blue powder obtained was analyzed by XRD, TEM, and HRTEM. Figure 1 shows the X-ray powder pattern obtained from the dark blue powder. Although it is difficult to match the powder pattern unambiguously to a specific phase among the various stoichiometric and nonstoichiometric tungsten oxide compounds and their rather similar structures,[38] the pattern is similar to that reported for $W_{18}O_{49}$ nanorods.[39] The corresponding powder pattern exhibits two sharp reflections (Figure 1); the diameter and intensities of these reflections point to highly ordered crystallites. The two reflections at 2θ 23.2° and 47.3° match best with the (010) and (020) reflections of the monoclinic phase

(24) Dumestre F.; Chaudret, B.; Amiens, C.; Respaud, M.; Fejes, P.; Renaud, P.; Zurcher, P. *Angew. Chem.* **2003**, *115*, 5132−5138; *Angew. Chem., Int. Ed.* **2003**, *42*, 5213−5216.
(25) Talapin, D. V.; Shevchenko, E. V.; Murray, C. B.; Kornowski, A.; Forster, S.; Weller, H. *J. Am. Chem. Soc.* **2004**, *126*, 12984–12988.
(26) Johnson, C. J.; Li, M.; Mann, S. *Adv. Funct. Mater.* **2004**, *14*, 1233–1239.
(27) Li, L. S.; Alivisatos, A. P. *Adv. Mater.* **2003**, *15*, 408–411.
(28) Sun, B. Q.; Sirringhaus, H. *J. Am. Chem. Soc.* **2006**, *128*, 16231–16237.
(29) Kim, F.; Kwan, S.; Akana, J.; Yang, P. D. *J. Am. Chem. Soc.* **2001**, *123*, 4360–4361.
(30) Artemyev, M.; Moller, B.; Woggon, U. *Nano Lett.* **2003**, *3*, 509–512.
(31) (a) Meuer, S.; Oberle, P.; Theato, P.; Tremel, W.; Zentel, R. *Adv. Mater.* **2007**, *19*, 2073–2078. (b) Zorn, M.; Meuer, S.; Tahir, M. N.; Khalavka, Y.; Sönnichsen, C.; Tremel, W.; Zentel, R. *J. Mater. Chem.* **2008**, *18*, 3050–3058. (c) Meuer, S.; Fischer, K.; Mey, I.; Janshoff, A.; Schmidt, M.; Zentel, R. *Macromolecules,* **2008**, *41*, 7946–7952. (d) Meuer, S.; Braun, L.; Zentel, R. *Chem. Commun.* **2008**, 3166–3168.
(32) Santato, C.; Odziemkowski, M.; Ulmann, M.; Augustynski, J. *J. Am. Chem. Soc.* **2001**, *123*, 10639–10649.
(33) Solis, J. L.; Saukko, S.; Kish, L.; Granqvist, C. G.; Lantto, V. *Thin Solid Films* **2001**, *391*, 255–260.
(34) Sayama, K.; Mukasa, K.; Abe, R.; Abe, Y.; Arakawa, H. *Chem. Commun.* **2001**, 2416–2417.
(35) Shengelaya, A.; Reich, S.; Tsabba, Y.; Müller, K. A. *Eur. Phys. J. B* **1998**, *12*, 13–15.
(36) (a) Rothschild, A.; Sloan, J.; Tenne, R. *J. Am. Chem. Soc.* **2000**, *122*, 5169–5179. (b) Therese, H. A.; Li, J.; Kolb, U.; Tremel, W. *Solid State Sci.* **2005**, *7*, 67–72. (c) Remskar, M.; Virsek, M.; Jesih, A. *Nano Lett.* **2008**, *8*, 76–80.
(37) Watchenrenwong, A.; Chanmanee, W.; de Tacconi, N. R.; Chenthamarakshan, C. R.; Kajitvichyanukul, K.; Rajeshwar, K. *J. Electroanal. Chem.* **2008**, *612*, 112–120 (see also references cited therein).
(38) Wells, A. F. *Structural Inorganic Chemistry*, 4th ed.; Clarendon Press: Oxford, 1975.
(39) (a) Frey, G. L.; Rothschild, A.; Sloan, J.; Rosentsveig, R.; Popovitz-Biro, R.; Tenne, R. *J. Solid State Chem.* **2001**, *162*, 300–314. (b) Seo, J. W.; Jun, Y. W.; Ko, S. J.; Cheon, J. *J. Phys. Chem. B* **2005**, *109*, 5389–5391.

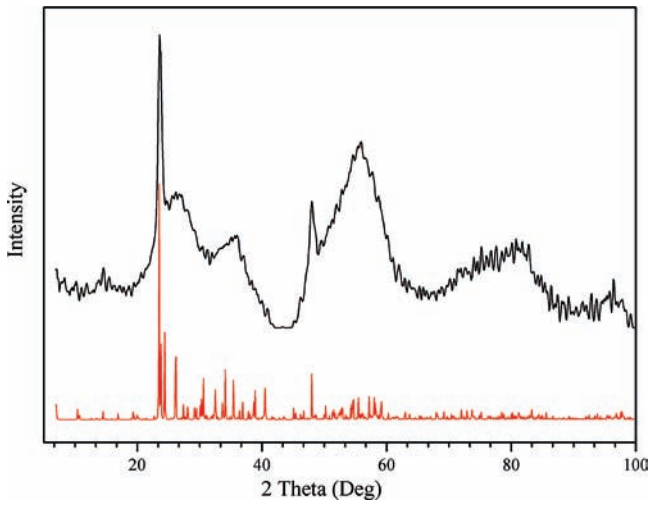

Figure 1. X-ray powder diffraction pattern (black line) of the reaction product. Red lines correspond to XRD pattern of $W_{18}O_{49}$ (JCPDS No. 36-101).

$W_{18}O_{49}$ ($WO_{2.72}$, JCPDS 36-101). All other reflections are much weaker, thus indicating a preferred orientation along the [010] direction. The crystal structure of $W_{18}O_{49}$ is strongly anisotropic and contains an ordered three-dimensional lattice of connected, edge-sharing, and corner sharing, mutually tilted WO_6 octahedra. The $W_{18}O_{49}$ structure was reported for tungsten oxide nanowhiskers and nanorods, where the growth also occurs along the short *b* axis.[41]

As the powder pattern is difficult to match unambiguously to a specific phase, X-ray photoelectron spectroscopy (XPS) measurements were carried out to find out the existence of $W_{18}O_{49}$ which has two different oxidation states. Figure S1 (Supporting Information) shows the W 4f core level spectra of the pristine (as-prepared) tungsten oxide nanowires. The measured spectrum can be deconvoluted into two doublets. The first doublet has the W $4f_{7/2}$ line at 31.4 eV and the W $4f_{5/2}$ line at 33.5 eV. The second doublet with very weak intensity has a lower binding energy with the W $4f_{7/2}$ line at 29.2 eV.

Tungsten oxide nanorods were structurally characterized by transmission electron microscopy (TEM). Samples were prepared by placing a drop of a dilute ethanolic dispersion of the nanorods on the surface of a 400 mesh copper grid backed with an amorphous carbon film and were dried. The nanorods obtained were uniform with an average diameter of 2 nm and length of 10 nm (Figure 2). The diameter is an order of magnitude smaller than that of previously reported tungsten oxide nanorods prepared by a variety of other methods. HRTEM enabled the imaging of planes, confirming the crystallinity of the nanorods. HRTEM also permitted the accurate measurement of the average nanorod thickness, found to be 2−2.2 nm (Figure 2).

Fourier transform infrared spectra exhibit the vibrations of an organic−inorganic hybrid structure. The nanorods prepared in the presence of surfactants exhibit a more complex IR spectrum (see Supporting Information, Figure S2). In the region of 1000−500 cm^{-1}, the bands characteristic for the W−O (950 cm^{-1}) units and the stretching vibrations of the bridging oxygen atoms O−W−O (600−780 cm^{-1}) appear.[40] The stretching vibrations due to the tungsten oxide framework in the range of 1000−500 cm^{-1} are split up and an unambiguous assignment of the bands is not possible. The feature bands in the range of 2940−2850 cm^{-1} are assigned to the $-CH_3$ and $-CH_2-$ stretching vibrations of the oleic acid and trioctylamine. Thermogravimetric analysis of the nanorods shows a weight loss of about 8% between room temperature and 500 °C (see Supporting Information, Figure S3). The results of the FT-IR spectroscopy and the TGA give clear evidence for a surface binding of the surfactants to the nanorods.

Optical Properties. Not much is known about the photoluminescence (PL) of tungsten oxide nanorods.[41] The room-temperature PL emission spectra of the tungsten oxide nanorods recorded at an excitation wavelength of 270 nm generally exhibit two emission maxima over the studied wavelength range, which is quite similar to a previously reported pattern for $W_{18}O_{49}$ nanorods, although the maxima of the two emission bands are less separated.[42]

The PL emission spectra measured in ethanol show an emission band at 3.14 eV (392 nm) and an additional blue emission band at 2.66 eV (465 nm). A similar PL spectrum with two emission maxima, yet at much lower energies of 2.8 and 2.3 eV, was observed previously for thin films of the related WO_3 system at 80 K, but the emission peak at higher energy (2.8 eV) disappeared at room temperature.[42] While the high-energy band was attributed to an electron−hole radiative recombination, the lower-energy band was assigned to localized states in the band gap due to impurities.[42b] The blue emission of the nanorods might originate from the presence of oxygen vacancies or defects; longer nanorods would possess more defects due to faster 1D crystal growth and thus a more intense PL emission associated with the concentration of defects. The

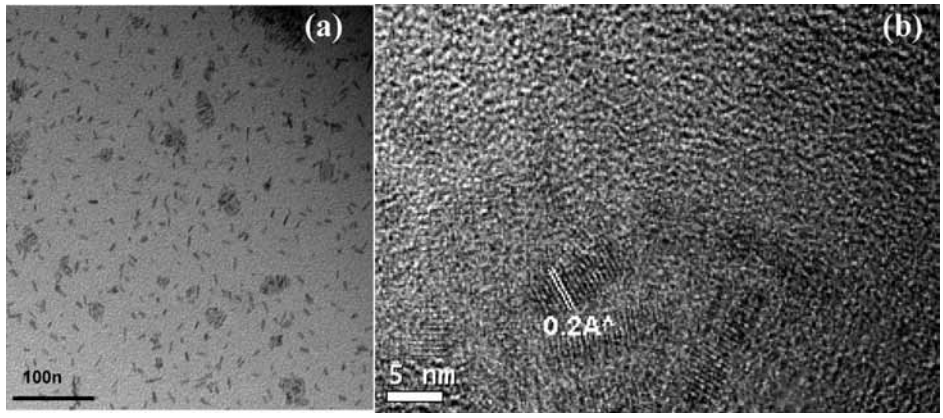

Figure 2. TEM (a) and HRTEM (b) images of the product obtained at 330 °C. The high resolution TEM (HRTEM) image shows that the nanorods are homogeneous with a diameter of 2 nm and a length of 8 nm.

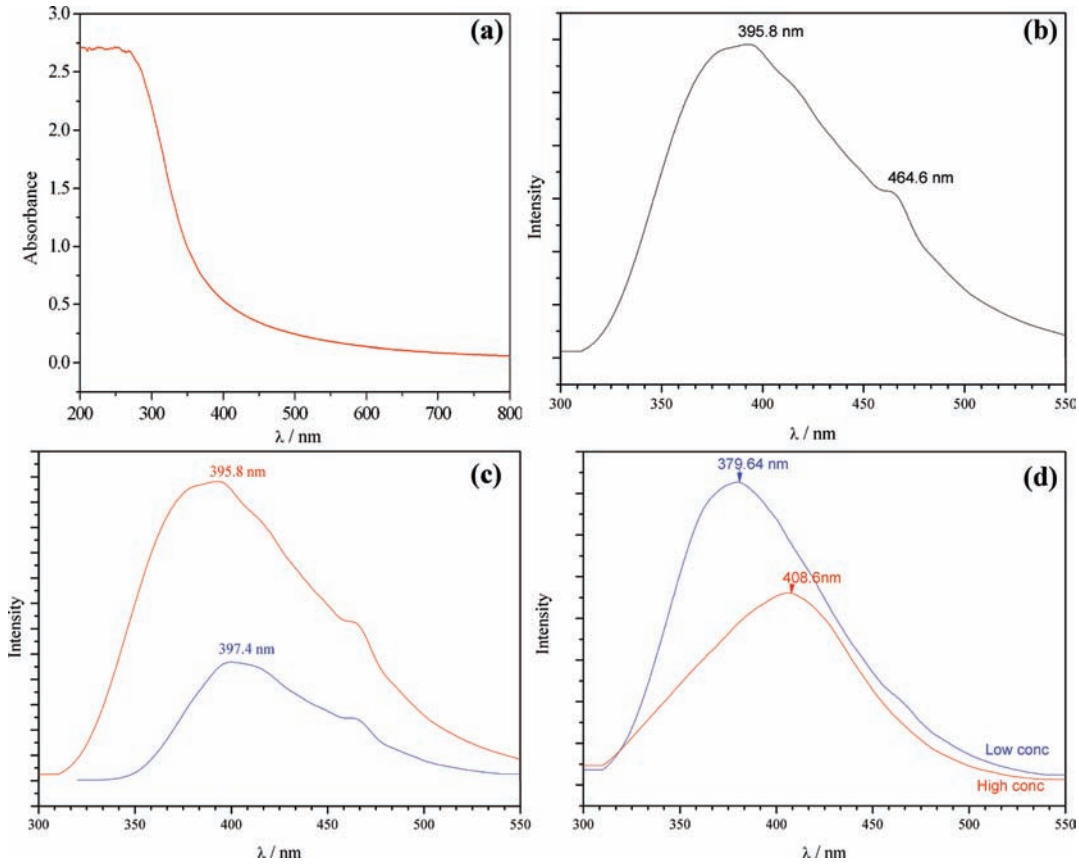

Figure 3. UV (a) and photoluminescence (b−d) spectra of the nanorods. (a) UV−vis spectrum of $W_{18}O_{49}$ nanorods in cyclohexane. PL was observed in ethanolic suspension (b) with two emission maxima at 395.8 and 464.6 nm. (c) PL obtained after modifying the surface with dodecanethiol (blue) in comparison with the ethanolic suspension (red). (d) PL obtained for the nanorods in cyclohexane with a concentration of 5 mg/mL (blue) and a concentration of 20 mg/mL (red), which shows a red shift in the emission maxima.

position of this blue emission peak does not show any size dependence, presumably because it is related to localized states in the electronic structure.

The optical properties were probed by varying the surface capping ligands (i.e, the thiol exchange). In a typical reaction, 0.01 g of tungsten oxide nanorods were dispersed in 5 mL of cyclohexane, 1 mL of dodecanethiol was added, and the mixture was stirred for 30 min at room temperature. Addition of ethanol and centrifugation resulted in the separation of the tungsten oxide nanorods, which were again redispersed in cyclohexane to measure the PL emission spectra. The PL emission spectra of the surface-modified nanorods are similar to those measured in ethanol; they show two emission maxima at 3.26 eV (392 nm) and 2.66 eV (465 nm), suggesting that the PL of the nanorods arise from quantum confinement rather than from surface defect states.

The nanorods were completely soluble in cyclohexane and formed a clear solution. PL emission spectra measured in cyclohexane revealed only one single emission maximum varying from 3.26 to 3.02 eV (380−410 nm) depending on the concentration of the nanorod solution. An increase of the concentration of the nanorods from 5 mg per mL of cyclohexane to 15 mg per mL of cyclohexane leads to a red shift of the emission (see Figure 3). This indicates a strong preference for self-assembly of the nanorods in cyclohexane that leads to size-dependent PL emission spectra depending on the concentration of the nanorods.

Self-Assembly. The tungsten oxide nanorods were found to have a strong preference for self-assembly. They were completely soluble in pure cyclohexane, pure chloroform, and a solvent mixture of ethanol and cyclohexane, forming clear blue solutions (see Supporting Information, Figure S5). When two solvents with different surface tensions were mixed, mass transfer in a liquid layer occurs due to the difference in the surface tension of the two liquids. Because a liquid with a high surface tension pulls more strongly on the surrounding liquid than one with a low surface tension, the presence of a gradient in surface tension will naturally cause the liquid to flow away from regions of low surface tension. The surface tension gradient can in turn be caused by a concentration or a temperature gradient. This effect is known as the Marangoni effect.[43] The presence of the surfactant in the liquid phase induces the appearance of a concentration gradient during the evaporation process. This results in a behavior similar to that of the temperature variation, ΔT.[44] The same kind of behavior can be

(40) Tocchetto, A.; Glisenti, A. *Langmuir* **2000**, *16*, 6173–6182.
(41) (a) Lee, K.; Seo, S. W.; Park, J. T. *J. Am. Chem. Soc.* **2003**, *125*, 3408–3409. (b) Niederberger, M.; Bartl, M. H.; Stucky, G. D. *J. Am. Chem. Soc.* **2002**, *124*, 13642–13643. (c) Lou, X. W.; Zeng, H. C. *Inorg. Chem.* **2003**, *42*, 6169–6171.
(42) (a) Manfredi, M.; Paracchini, G. C.; Schianchi, G. *Thin Solid Films* **1981**, *79*, 161–166. (b) Paracchini, C.; Schianchi, G. *Phys. Status Solidi A* **1982**, *72*, K129–132.
(43) (a) Marangoni, C. *Ann. Phys.* **1871**, *143*, 337–354. (b) Moussy, C.; Lebon, G.; Margerit, J. *Eur. Phys. J. B* **2004**, *40*, 327–335. (c) Cerisier, P.; Porterie, B.; Kaiss, A.; Cordonnier, J. *Eur. Phys. J. E* **2005**, *18*, 85–94.

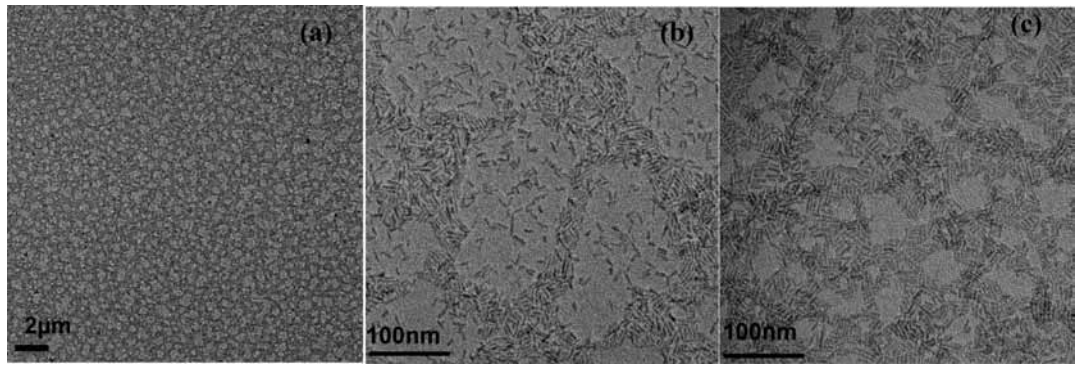

Figure 4. TEM images of the mesostructures obtained when tungsten oxide nanorods were drop casted from chloroform solution. (a) Low resolution overview image showing the mesostructures. (b,c) TEM images showing the mesostructures at concentrations of 4 mg/mL (b) and 8 mg/mL (c) of chloroform.

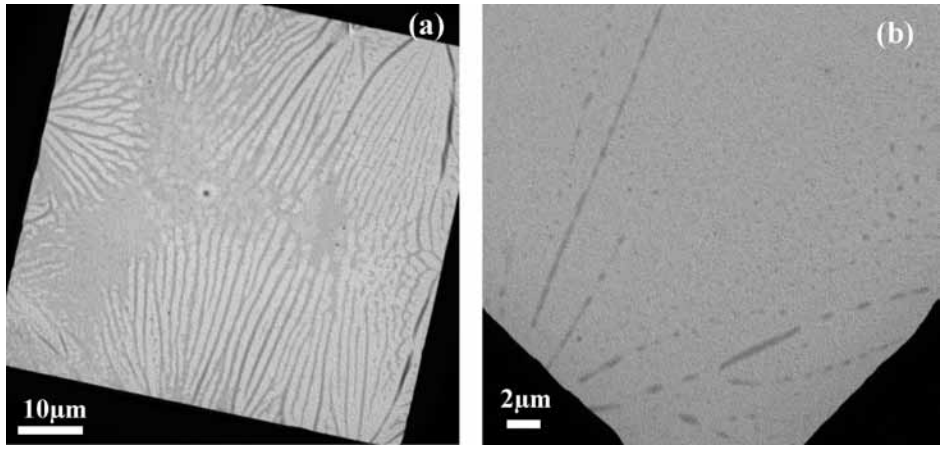

Figure 5. Low resolution TEM images of the linear tracks obtained at concentrations of (a) 12 and (b) 2 mg/mL in cyclohexane.

observed with surfactant-coated nanorods instead of surfactants alone. When the liquid film is thick enough, the gravitational field also plays a role and generates Rayleigh buoyancy-driven convection.[45] If the liquid film is very thin or the interface tension is very low, it is denoted as long wavelength Marangoni instability.[46] This appears when the film thickness is in the same range as the convection and generates long-range deformation of the surface that in turn can lead to film rupture by a hole nucleation process. It is especially relevant for the drying of thin films, as in the present study.

The nanorod solutions were drop casted onto a carbon-coated TEM grid. Transmission electron micrograph images show the typical superstructures formed when nanorods are deposited on a carbon-coated TEM grid from the solution by slow solvent evaporation. Interestingly, the superstructures obtained from all three solvents were different. These different superstructures are assumed to be a result of the slow evaporation of the solvent on the TEM grid and the different polarity and wetting behaviors of the solvents on the carbon-coated TEM grid.

First the behavior of tungsten oxide nanorods was studied in the moderately polar aprotic solvent chloroform in which the tungsten oxide nanorods were completely soluble as a blue-colored solution. Figure 4 shows TEM images obtained from a solution containing 4 mg of tungsten oxide nanorods dissolved in 1 mL of chloroform. As shown in Figure 4a, the nanorods form complex organized arrangements consisting of close-packed structures. Arrays of hexagonal patterns as shown in Figure 4b are observed. The dark "walls" in Figure 4a correspond to nanorod aggregates, whereas the bright regions correspond to low particle density areas. The formation of these mesostructures indicates a possibility for preparing layers of ordered tungsten oxide nanorods on substrates, which may be useful for gas sensors or in optical applications. Increasing the concentration of the nanorods to 8 mg/mL in chloroform did not lead to significant changes in the mesostructures except that they were more densely packed (see Figure 4c). These patterns are similar in shape to those observed by Pileni et al.[47] for concentrated silver and by Korgel et al.[48] for gold nanocrystal solutions. This pattern formation was attributed in both cases to the Marangoni effect. The regularity of the hexagonal patterns depends on the orderliness of the instability fingerings at the contact line. The inter-ring spacing (λ) corresponds to the characteristic wavelength of the Marangoni instability by $\lambda = 2\pi h/R$, where h is the film thickness of the condensed water layer and R is the dimensionless periodicity of the convection.[49] This is consistent with theories where a concentration gradient induces an increase in the Marangoni number and consequently an increase in the instabilities, such as that observed for a temperature gradient. When pure cyclohexane was used as a solvent, only linear tracks were observed as shown in Figure 5.

(44) Fanton, X.; Cazabat, A. M. *Langmuir* **1998**, *14*, 2554–2561.
(45) Rayleigh, L. *Philos. Mag.* **1916**, *32*, 529–546.
(46) (a) Oron, A.; Davis, S. H.; Bankoff, S. G. *Rev. Mod. Phys.* **1997**, *69*, 931–980. (b) VanHook, S. J.; Shatz, M. F.; McCornick, W. D.; Swift, J. B.; Swinney, H. L. *Phys. Rev. Lett.* **1995**, *75*, 4397–4400.
(47) Maillard, M.; Motte, L.; Ngo, A. T.; Pileni, M. P. *J. Phys. Chem. B* **2000**, *104*, 11871–11877.
(48) Stowell, C.; Korgel, B. A. *Nano Lett.* **2001**, *1*, 595–600.
(49) Maillard, M.; Motte, L.; Pileni, M. P. *Adv. Mater.* **2001**, *13*, 200–204.

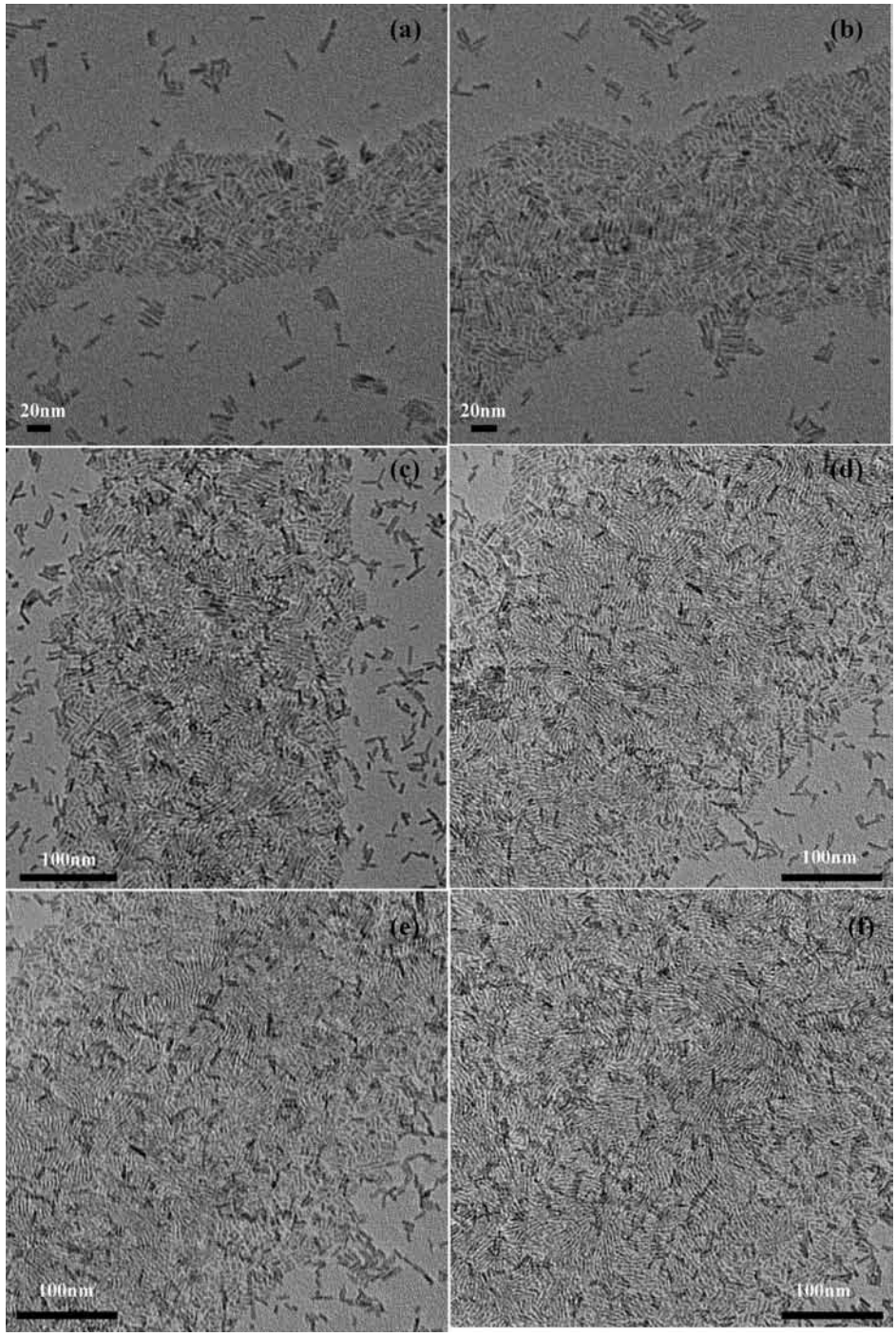

Figure 6. TEM images of mesostructures obtained by drying of solutions containing tungsten oxide in cyclohexane in concentrations of (a) 2, (b) 4, (c) 6, (d) 8, (e) 10, and (f) 12 mg/mL.

In the next step, the role of the nanorod concentration for the formation of the liquid crystalline phases was considered. When the concentration of the tungsten oxide nanorods was lowered to 2 mg/mL of cyclohexane, the 1D framework collapsed completely. Therefore, we assume the critical concentration of the tungsten oxide nanorods in cyclohexane to be between 2−4 mg/mL for obtaining the assembled structure. At a concentration of 2 mg/mL (Figure 6a), only a few 1D linear tracks were obtained, and a 2D assembly in areas of 40−60 nm was observed. Most of the nanorods are still aligned side by side, but the area of alignment was much smaller. The results imply that the solvent and surfactants surrounding the tungsten oxide nanorods might play an important role in the formation of the self-assembled superstructures. Therefore, the interaction between the alkyl groups of surfactants and solvent might function as the direction controlling agent.

Upon increasing concentration of the tungsten oxide nanorods from 2 to 12 mg/mL cyclohexane, similar 1D tracks were observed over micro- to millimeter-sized areas, as shown in Figure 6. The diameter and the length of these linear tracks increased with increasing concentration of the nanorods. An increase of the concentration of the nanorods led to the formation of liquid crystalline phases along the diameter of the 1D tracks.

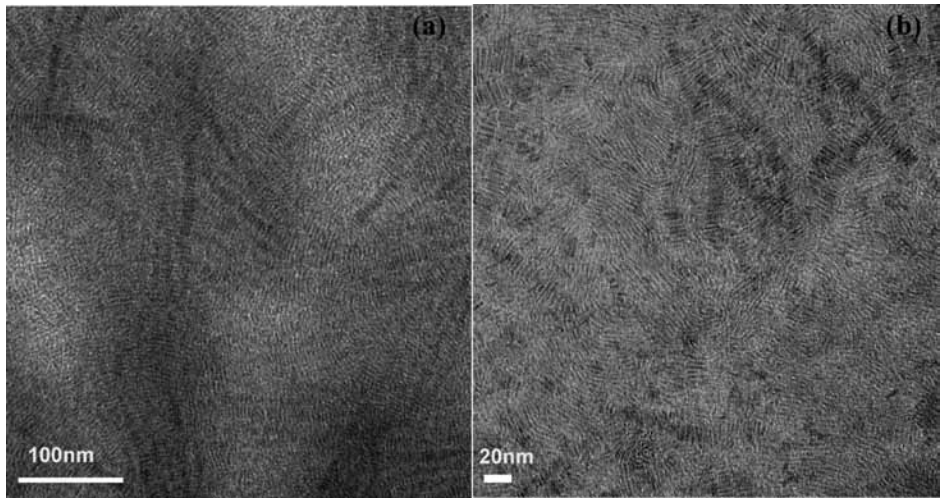

Figure 7. TEM images of linear tracks formed for concentrations of 25 mg/mL cyclohexane. (a) Multilayer formation of the nanorod tracks; (b) the top layer of the nanorods has both positional and orientational order and also positional ordering in longitudinal direction (smectic A type of ordering), whereas the bottom layer exhibits only orientational but no positional ordering (nematic ordering).

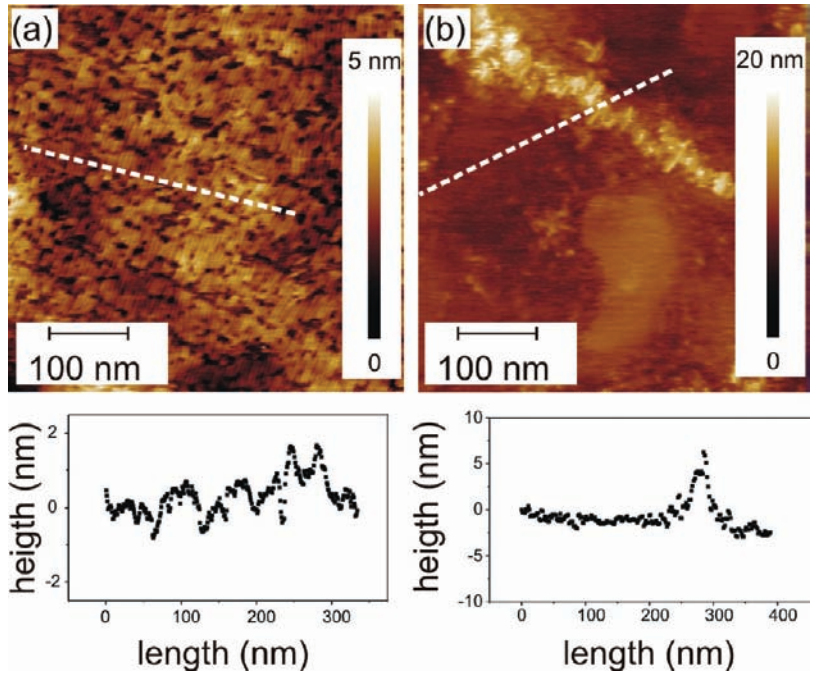

Figure 8. SFM images obtained when the nanorods were dip-coated on freshly cleaved mica into solutions for concentrations of (a) 10 and (b) 25 mg/mL. The length scales for the images are 500 × 500 nm square, also hoch zwei (a) and 800 × 800 nm hier auch hoch 2 (b), and the corresponding height profiles along the line drawn.

Figure 6 shows TEM images obtained for different concentrations of tungsten oxide nanorods. As shown in Figure 6a,b, the tungsten oxide the nanorods were aligned side by side for concentrations of 2 and 4 mg/mL. For concentrations higher than 7 mg/mL schlieren textures appeared within the 1D tracks (Figure 6c−f), and nematic liquid crystalline phases began to form. For a concentration of 25 mg/mL cyclohexane, the diameter of the linear tracks increased to micrometer size and on each of the linear tracks multilayers of tungsten oxide nanorods were observed, as shown in Figure 7.

Transmission electron microscopy revealed that the nanorods formed multilayers using a solution with concentration of 25 mg/mL (Figure 7a). The bottom layer of the nanorods appear to have only orientational but no positional ordering (nematic liquid crystalline ordering), whereas the top layer of the nanorods has both positional and orientational ordering with positional ordering in longitudinal direction similar to a smectic A type of arrangement. The multilayer formation could be observed by scanning force microscopy (SFM) as well. A freshly cleaved mica sheet was dipped in a solution of tungsten oxide nanorods having concentrations of 12 and 25 mg/mL. Interestingly, when the nanorods were dip-coated on freshly cleaved mica, a thin film of the nanorods was observed on the substrate with different domains (Figure 8a). Even though the nanorods formed a thin film on the mica substrate (Figure S6, Supporting Information) with increasing concentration of the tungsten oxide nanorod solution, multilayer formation was observed (Figure 8b). The corresponding height profile along the dashed line (Figure 8b) shows the formation of bi- or multilayers for high concentrations. The measured height differences in (a) are around 2 nm, as expected from the diameter of the nanorods. The measured

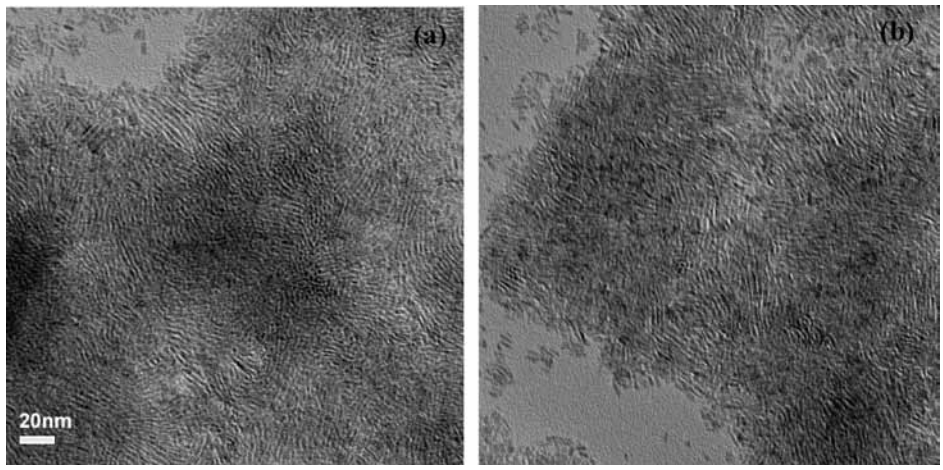

Figure 9. TEM images of the superstructures formed from a solvent mixture of ethanol and cyclohexane in a 1:1 ratio.

increase in roughness to values > 4 nm (b) is compatible with the formation of bi- or trilayers.

Self-Assembly from Solvent Mixtures. In the next step, the aggregation behavior from a solvent 50:50 mixture of ethanol and cyclohexane was studied. Upon evaporation, one solvent will evaporate first owing to its higher vapor pressure. The nanorods bundle into separate 2D close-packed stacks (Figure 9) where they align side by side. Increasing the concentration led to an increase of the area of the 2-D close-packed stacks. When two liquid surfaces are formed by intermolecular forces, which are unbalanced at the boundary, a surface tension is generated. When liquid layers with different surface tension get in contact, these forces cause a flow due to a local difference in the surface tensions of the liquid. The 2-D close packed stacks shown in Figure 9 could be the result of the Marangoni flow driven by the surface tension gradient between the two solvents. For a 50:50 mixture of ethanol and cyclohexane, the drying kinetics was found to be dominated by the ethanol, and 2-D stacks of the nanorods were formed upon drying.

When the mixing ratio was changed from 1:1 to 1:2 (see Figure 10), two types of superstructures were formed. The nanorods self-assemble at a micrometer scale to form 2D areas and 1D linear tracks. The 1D linear tracks the nanorods exhibit positional and orientational order (Figure 10b), whereas the 2D areas next to the 1D linear tracks were found to have only orientational but no positional order (Figure 10c,d).

The different levels of the ordering on the grid can be attributed to inhomogeneities in the local concentration of the nanorods and the nonequilibrium solvent drying kinetics. Two parallel processes can occur during the preparation process. (i) Because of the local difference in the surface tension generated as a result of the intermolecular forces, the forces cause a flow, and it is especially strong for solutions of the nanorods in mixed solvents and the patterns obtained as a result of the local difference in the surface tension are called "breath figures". (ii) The evaporation of the solvent leads to lateral structure formation on the micrometer to millimeter scale. With increasing concentration upon drying the solvent, the nanorods organize into a LC-phase. Thus, the different levels of ordering of the nanorods on the grid can be attributed to a flow of the solvent mixture due to a local difference in the surface tension.

Formation Mechanism of the Different Superstructures. To find out the mechanism behind the formation of the stripes in the case of cyclohexane, contact angle measurements were carried out with a solution of 8 mg/mL of nanorods dissolved in cyclohexane on a mica plate coated with a 5 nm carbon film. We considered 5 nm carbon coated mica to be equivalent to a TEM grid. In the case of this carbon coated mica substrate, the contact angle for the solvent cyclohexane was found to be 4°, that is, the carbon-coated mica substrate had a very low contact angle of 4° and hence may be considered a wettable substrate. As the surfactant-coated nanorods/cyclohexane suspension recedes on a wettable substrate during evaporation, the condensed cyclohexane near the contact line wets the substrate completely and produces a very thin cyclohexane film. Due to this surface tension gradient between the solvent cyclohexane and the receding surfactant coated nanorods and the fingering instability at the receding contact line, the nanorods suspension quickly moves toward and into the fingers and facilitates the growth of fingers into stripes. As cyclohexane is a rapidly evaporating solvent surrounding the stripes, the surfactant-coated nanorods form ordered stripes. On a glass substrate or a silicon wafer with a native oxide layer, the contact angle for cyclohexane was found to be 20°. Interestingly, on a nonwettable substrate, that is, a silicon wafer, no stripe formation occurred and coffee stain patterns were formed. These observations suggest that both coffee stain and stripe patterns are formed, depending on the wettability of the substrates. The laser microscope images (Figure S7, Supporting Information) show that the condensed solvent consisting of nanorods self-assembles into a different pattern.

To explain the observed difference in the self-assembled patterns in different solvents, we derived a quantitative model to analyze the surface energy in solution.[50] In the Supporting Information we present a theoretical estimate of this change of the surface potential based on the experimentally determined contact angles and surface tensions. The driving force for the nanorod segregation to the surface can be estimated by calculating the difference of surface potential Φ_t between a nanorod completely immersed in solution and a nanorod segregated to the surface and exposing a portion of its surface to air. The analysis shows that only in the case of cyclohexane the change of the surface potential upon exposing the end of the nanorod to the surface is negative, whereas it is positive in all the other cases. Hence, the nanorods tend to be immersed in the solvent in the case of cyclohexane whereas the nanorods tend to segregate on the surface in all other cases. During evaporation the solvent molecules move toward the interface from the interior to replenish the surface liquid, and the surface moves toward the substrate. At the same time, nanorods diffuse into the solution for

(50) Sun, B.; Sirringhaus, H. *J. Am. Chem. Soc.* **2006**, *128*, 16231–16327.

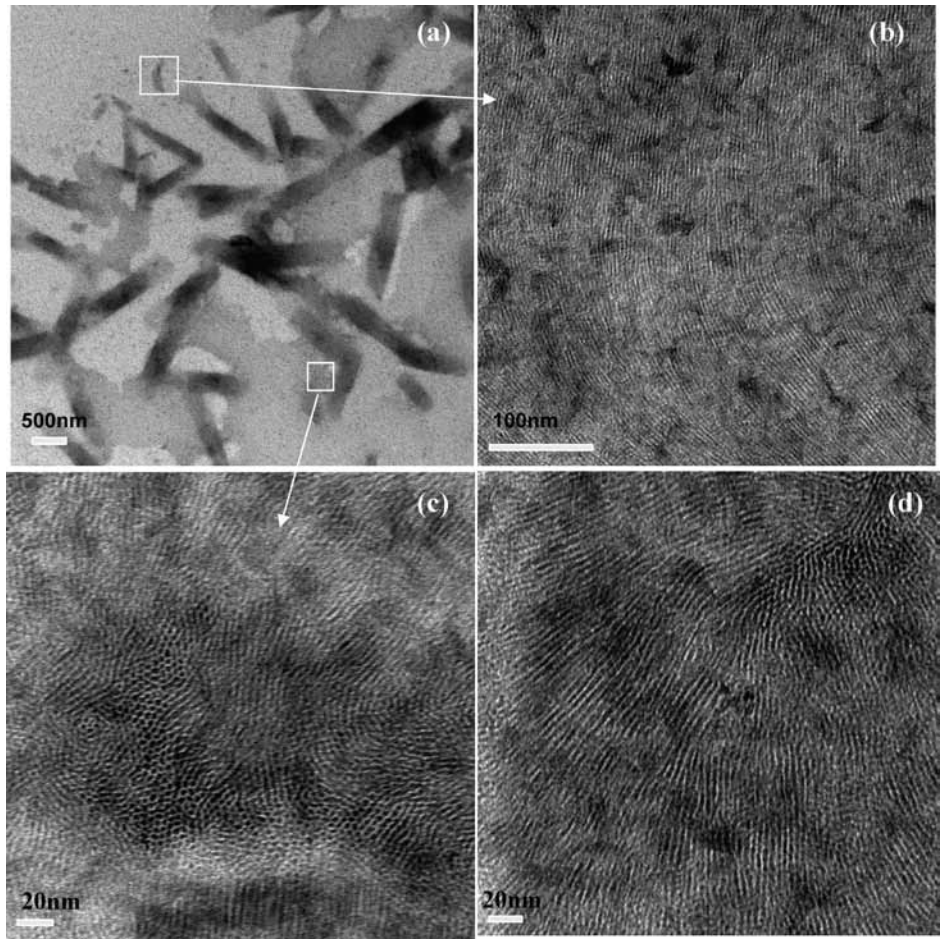

Figure 10. TEM images showing the assembly of the nanorods drop casted in a solvent mixture of ethanol and cyclohexane in 1:2 ratio. (a) Low resolution TEM image showing different types of superstructures formed: (b) structures in which nanorods have both orientational and positional order; (c) honeycomb-like structure showing an area with a liquid crystalline nanorod phase with nematic order collapsing (d) on the substrate without much rearrangement to structures where the nanorods have an orientational order but random positions.

cyclohexane, whereas the nanorods tend to be at the surface rather than diffusing along with the solvent in all remaining cases. We postulate that, as a result of its lower surface tension (indicated by the contact angle), the tungsten oxide nanorods have a stronger tendency to segregate at the liquid/air interface in cyclohexane. The surface potential of the nanorods is with a value of $5.399\pi R^2$ highly positive for the 1:1 solvent mixture of cyclohexane/ethanol. This indicates that the nanorods prefer to segregate at the surface rather than diffusing along with the flow. This could explain the formation the 2D patterns in the case of the 1:1 cyclohexane/ethanol mixture. For the 2:1 mixture of cyclohexane/ethanol a positive value of $0.6256\pi R^2$ was obtained.

Apart from the wetting behavior of the solvents, two other types of interactions might play a dominant role in the formation of the mesostructures: (i) van der Waals attraction between the nanorods and (ii) dipole−dipole interactions between the solvent and the surfactant layer attached to the nanorod surfaces.

Liquid Crystal Formation on Supports versus Aggregation in Solution. The formation of liquid crystalline phases of tungsten oxide nanorods was verified by examining the birefringence of the nanorods by placing the solution on a coverslip in a polarized light microscope with crossed polarizers. Figure 11 shows the birefringence observed under the polarized light microscope during evaporation of the solvent. Figure 12 shows a flat channel capillary that was filled with the nanorod solution and allowed to dry. While the solvent evaporated, the nanorods formed a lyotropic liquid crystalline phase. The orientational order of the liquid crystals is maintained during the evaporation of the solvent. As a result, the nanorods form a birefringent phase. The birefringence is directionally dependent as shown by turning the polarizer pair. This demonstrates that a macroscopic orientation of the nanorods over more than 100 μm can

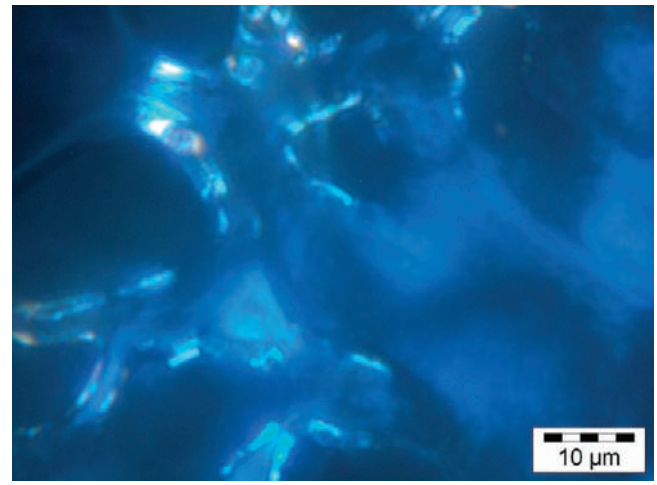

Figure 11. Birefringence observed under a polarized light microscope during evaporation of the solvent. The blue background is blue due to the absorption of tungsten oxide nanorods.

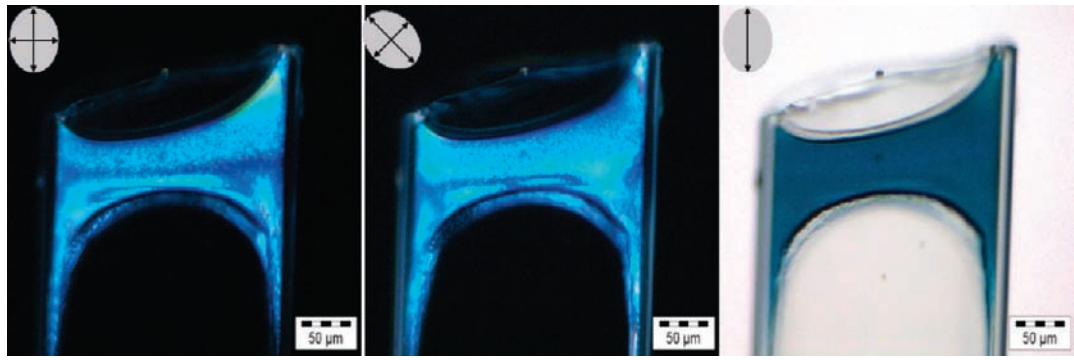

Figure 12. Birefringence observed in polarized light during the evaporation of the solvent. The blue background is due to the absorption spectra of tungsten oxide nanorods.

be achieved. For comparison, also a normal microscope image of the same area is given showing the blue adsorption of the nanorods without crossed polarizers (Figure 12c).

To further understand the origin of the tungsten oxide nanorod superstructure assembly, we checked for NR ordering in solution. SAXS measurements were carried out for solutions of the NRs in cyclohexane with concentrations between 2 and 20 mg/mL (as used for the TEM studies). The corresponding SAXS patterns (see Figure S8, Supporting Information) did not show any maxima, which points to the absence of significant preformed aggregates in solution for this concentration regime. These SAXS measurements suggest that, even at concentrations of 20 mg/mL, ordered aggregates do not form in solution but only on solid supports upon evaporation of the solvent.

Conclusions and Outlook

In conclusion, we developed a soft chemistry route for the synthesis of the tungsten oxide nanorods. These nanorods were found to self-assemble in organic solvents like chloroform, cyclohexane, and mixtures of cyclohexane and ethanol. For each individual solvent, a different ordering pattern was observed; the formation of these different superstructures is related to the interactions between the nanorods, which is mediated by the polarity of solvent molecules and the nanoparticle concentration, which is dictated by the vapor pressure of the solvent.

With chloroform the formation of nanorod mesostructures was observed, which began to compact upon increasing concentrations. With pure cyclohexane as solvent, 1D stacks of nanorods were obtained with lengths of several micrometers. Increasing the concentration of the nanorods led to an increase in the diameter of the 1D stacks. The formation of schlieren textures was observed above a threshold concentration of 7 mg/mL of cyclohexane. The critical concentration for a transition from the isotropic to the nematic phase was estimated to be around 4 mg/mL of cyclohexane. Increasing the concentration to 25 mg/mL lead to the formation of micrometer-sized 1D linear stacks and finally to the formation of multilayers with a smectic kind of organization. The organization was found to follow the "Benard−Marangoni effect" because of the local surface tension gradient resulting in the formation of "Breath Figures".

Although the bundling of 1D semiconductor nanostructures has been theoretically predicted and experimentally observed,[4] well-aligned arrays of nanorods without an external direction-controlling force, for example, by evaporation in the presence of ordered substrate, are rare examples. Recently, CdS nanorods (≈5 nm in diameter and ≈15 nm in length) with surface bound tri-*n*-octylphosphine (TOP) and tetradecylphosphonic acid (TDPA) were reported to form arrays of self-bundled rods in the absence of an external force. Here, the increasing concentration of the nanorods upon evaporation of the solvent and the decrease of their interfacial energy caused by interlacing the alkyl chains of surfactants seem to be a driving force for their organization.[51]

Understanding the role of the detergents and the solvents in the formation of the ordered arrays of the tungsten oxide nanorods requires further investigation. The roles of the nanorod dimensions, the particle−particle and particle−solvent interactions, and the local concentration gradients are still unclear. Further studies on the underlying self-assembly mechanism using the techniques such as cryo-TEM are in progress. Once achieved, such understanding will open up new possibilities for the processing of nanoscopic building blocks into the desired structures. We assume that ordered arrays of the type presented here may be used for sensor layers or for templating the preparation of nanometrically thin layers of materials into mesoscopic architectures to meet the emerging needs of advanced technologies.

Acknowledgment. The authors would like to acknowledge Dr. Enrico Mugnaioli, Daniel Kessler, Stefan Frank, Chandra M. Rao Volla, and Siham Ouardi for help with the EDX analysis, contact angle measurements, laser microscopy, quantitative analysis, and XPS measurements, respectively. This work was supported by the Deutsche Forschungsgemeinschaft (DFG) within the IRTG "Self-Organized Materials for Optoelectronics". A.Y. and S.M. are recipients of fellowships from POLYMAT, the Graduate School of Excellence of the State of Rhineland-Palatinate and the Verband der Chemischen Industrie (VCI). We are indebted to the Center for Electron Microscopy (EZMZ) for access to its facilities and the Materials Science Center (MWFZ) in Mainz for support.

Supporting Information Available: (1) XPS spectra of the tungsten oxide nanorods, (2) vibrational spectra of functionalized nanorods, (3) thermogravimetric analysis of the nanorods, (4) excitation and emission spectra of the nanorods, (5) optical image of the tungsten oxide nanorods in solution, (6) SFM images of the nanorods dip-coated on mica plates, (7) laser microscope images on silicon wafer and carbon coated mica, (8) SAXS data for a solution of nanorods in a capillary and for the powder sample, and the quantitative analysis of the surface and interfacial tensions. This material is available free of charge via the Internet at http://pubs.acs.org.

JA9007479

(51) (a) Ahmed, S.; Ryan, K. M. *Nano Lett.* **2007**, *7*, 2480–2485. (b) Kang, C.-C.; Lai, C.-W.; Peng, H.-C.; Shyue, J.-J.; Chou, P.-T. *ACS Nano* **2008**, *2*, 750–756.